Core-shell model of the vacancy concentration and magnetic behavior for antiferromagnetic nanoparticle

Suman Mandal, S. Banerjee, and Krishnakumar S. R. Menon*
Surface Physics Division, Saha Institute of Nuclear Physics, Kolkata 700064, India
(Received 31 August 2009; revised manuscript received 26 October 2009; published 22 December 2009)

The local defect structure of NiO nanoparticles was determined by extended x-ray absorption fine structure method. By using the bulk and surface sensitive characterization techniques, we are able to show that the vacancies mostly reside on the surface of the particles and the distribution of vacancies can be considered within a core-shell model. We argue that these observations can give a suitable explanation for the venerable problem of observed magnetic behaviors of antiferromagnetic nanoparticles and other functional properties of the material. The observed magnetic moment has been attributed to the interacting vacancies inside the antiferromagnetic host and the distribution of vacancies over the particle volume determines behaviors such as size-dependent different nature of spin-glass freezing and exchange bias.

DOI: 10.1103/PhysRevB.80.214420 PACS number(s): 75.75.+a, 61.72.jd, 78.70.Dm, 75.50.Ee

I. INTRODUCTION

In recent years, functional materials in nanoparticle form have been actively studied due to both scientific interests and potential applications. Nickel oxide (NiO) is a very prosperous material extensively used in catalysis, battery cathodes, gas sensors, electrochromic films, and magnetic materials.[1–5] Recently, reversible resistance switching has been found to take place, signaling the possibility of nanoscale resistance memory devices,[6] and also the use of NiO as hole-transporting layer in quantum-dot light-emitting devices has been demonstrated.[7] The performance of these devices strongly depend on the stoichiometry or preparation condition of the material. The general chemical formula of nickel oxide is Ni_xO_y. The values of (x,y) can be changed by changing the synthesis conditions. NiO is known to be *p*-type semiconductor and usually has an oxygen excess coming from the Ni vacancies in the system. First-principles thermodynamical calculations[8–10] also show that Ni vacancy is the most dominant point defect present in the system, rather than the absolute oxygen excess or oxygen interstitial, which are also supported by the present experimental findings.[11–13] The another most important issue is the distribution of vacancies over the particle volume. It is expected that the defect formation energy near-surface region and in the bulk of the particle will be different due to various uncompensated natures on the surface. This specific vacancy distribution has its strong effect on the overall electrical, electronic, and magnetic properties of the material, which has never been explored as a direct experimental finding. For the case of nanoparticle, the defect chemistry is expected to be considerably different than that of bulk under similar preparation condition with ambient atmosphere due to very large surface contribution and can have interesting material properties compared to bulk.

In this context of the discussion, we will specifically consider the magnetic properties of NiO nanoparticles demonstrating the general importance of the vacancy distribution over the particle volume, as an example. In the present decade or so, efforts have been devoted to explore the unexpected observed magnetic properties in both nonmagnetic[14–28] and magnetic[29–39] nanoparticles. To date, the mostly accepted model is the vacancy induced magnetism (specially ferromagnetism) for the case of nonmagnetic systems through various experimental and theoretical studies, as cited above. The issue of antiferromagnetic nanoparticles is rather more interesting because of its magnetically compensated nature and presence of active magnetic interactions, unlike to the case of nonmagnetic systems. As a matter of fact, one should not expect any net magnetic moment in antiferromagnets but historically, a finite magnetic moment has been observed for small antiferromagnetic particles. The exact origin remains unresolved, till now. The idea of Neel (1961) regarding the permanent magnetic moment of antiferromagnetic nanoparticle due to uncompensated surface spins of the "two sublattices" was expanded to a "multisublattice" model to explain the observed larger magnetic moment as expected from two-sublattice model, by Kodama *et al.*[29] in 1997, through many unsolved questions raised regarding the validity of Neel's two-sublattice model in contemporary literatures.[30] More recently, the observation of the spin-glass behavior in many antiferromagnetic nanoparticle systems along with loop shift upon field cooling, large magnetic moment and interestingly the absence of spin-glass behavior in many nonmagnetic nanoparticles[40] has established the fact that, spin-glass nature must be a unique feature of antiferromagnetic nanoparticle systems and this classifies two broad group of systems in their nanomagnetism. It seems that these observations cannot be explained by proposed multisublattice model. Recently some groups have reported that it can be considered as a core-shell exchange bias system where shell is ferromagnetic or spin-glasslike or diluted antiferromagnet.[36,39,41] In this model, loop shift can be explained as a result of interfacial coupling between shell (spin glass or FM) and core (antiferromagnet).[35,39] In some literature, the magnetism was attributed to the presence of higher oxidation state (Ni^{3+}) in NiO lattice, which is responsible for the observed magnetic moment.[42] Even recently, the presence of Ni^{3+} ions in NiO has been shown.[11] Sometimes, the enhanced catalytic properties of NiO nanoparticle has been attributed to the presence of Ni^{3+} ions.[43] However, some studies[44,45] indicate the presence of only Ni^{2+} ions. The issue

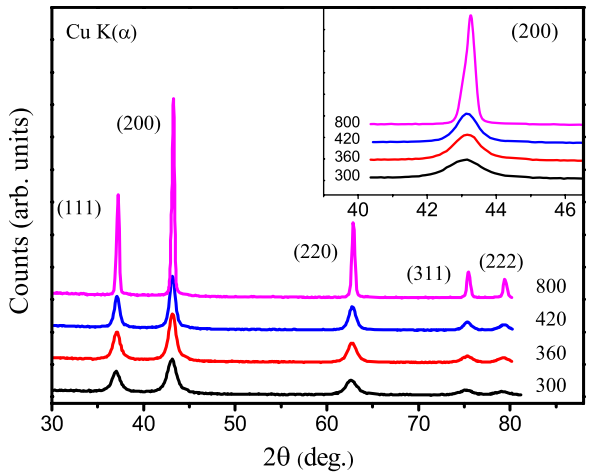

FIG. 1. (Color online) XRD pattern of NiO nanoparticles prepared at different temperatures (in degree Celsius) as indexed with Cu $K(\alpha)$ radiation (main panel). The zoomed view of (200) peak is shown in inset.

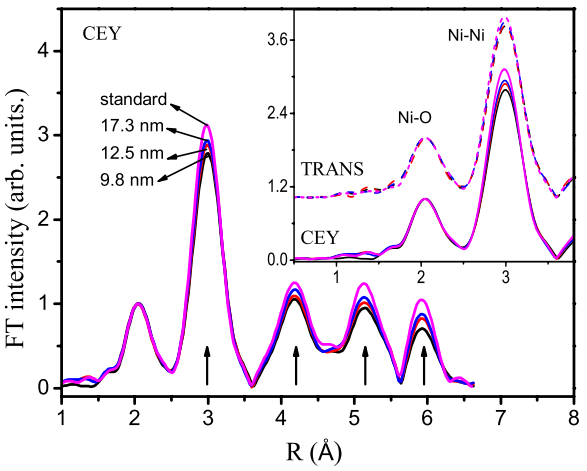

FIG. 2. (Color online) The particle size dependence of FT intensity in CEY mode (main panel). Comparison of the data of CEY mode with TRANS mode (inset).

of the vacancy induced oxidation state and consequently its effect on magnetic (also other material properties) deserves some more work. So, in the present status of understanding, the magnetic behaviors (and specially their origin) of antiferromagnetic nanoparticles remain controversial, contributed by studies mostly based on magnetization measurements. The evidence of vacancy induced magnetism in nonmagnetic systems suggests that vacancy can play a vital role for antiferromagnetic nanoparticles also, which has already been indicated in recent literatures.[38,46]

II. TECHNICAL DETAILS

To address these issues, regarding distribution of vacancies over particle volume, vacancy induced oxidation state, and effects on magnetic properties, we have performed a detailed local structure characterization by extended x-ray absorption fine structure (EXAFS) and electronic structure by XANES (x-ray near-edge absorption spectroscopy) at metal edges. For this purpose, we have prepared the nanoparticles by decomposing the chemically precipitated nickel hydroxide at various temperatures because this method has been widely used in relevant studies.[29,30,33,39] The magnetic properties have been characterized by superconducting quantum interference device magnetometer. From the x-ray diffraction (XRD) data as shown in Fig. 1, we see the formation single phase NiO nanoparticles with preparation temperatures (in degree Celsius) as indexed. The average particle sizes as estimated from the line broadenings are 9.8 nm (300 °C), 12.5 nm (360 °C), and 17.3 nm (420 °C). The sample prepared at 800 °C with large grain size (about 200 nm, from transmission electron microscopy image) is chosen to be standard. We should mention that XRD gives an estimation of average particle size which is often reasonable for smaller particle size.

The x-ray absorption spectra were collected at the XAFS (BL 11.1) and BEAR (Bending Magnet for Emission Absorption and Reflectivity) (BL 8.1 L) beamlines at Elettra Synchrotron Center, Italy. The energy scale has been calibrated by measuring the absorption through a Ni foil. The energy of the first inflection point of Ni K edge of Ni foil is taken to be 8331.53 eV. The data have been acquired in both bulk sensitive transmission (TRANS) mode and near-surface sensitive (due to an exponential decaying behavior of the signal with the depth from the sample surface[47]) conversion electron yield (CEY) mode[48] where the samples were surrounded by He gas at atmospheric pressure. We use CEY mode because of higher signal intensity compared to total electron yield (TEY) mode, with reasonable near-surface sensitivity.[49] By the combination of these two techniques, we can separate out the bulk and near-surface contributions of the relevant parameters. The Ni L_{23} x-ray absorption spectroscopy measurements have been performed with TEY mode. The background removal, normalization of the data have been performed by following the standard procedures using Athena.[50] The structural refinement[51,52] is carried out by using DL-excurv code[53] from Daresbury Laboratory. In this code, the effect of multiple scattering can be considered by calculating all of the multiple-scattering paths within a cluster centered around the central atom. The fitting is carried out in the R [Fourier transformed (FT)] (Ref. 54) space, with k range chosen from 3.5 to 15 Å^{-1}. The k^3 weighting is used to include high energy part of the oscillation. The fitting is performed on the first two cells, that is, on the first two peaks in the R space which is sufficient to get information about the coordination numbers and bond lengths.

III. RESULTS AND DISCUSSIONS

A. Core-shell model of vacancy concentration

In Fig. 2, we show the spectra in R space for different nanoparticles in both TRANS and CEY modes. Before we go to the fitting procedure, we would like to discuss about different features as can be extracted qualitatively. A careful inspection reveals that FT intensity decreases for all the Ni coordination cells (indicated by arrows in figure) as the particle size decreases. Since this intensity gives an estimation

TABLE I. Second cell population (N_2) and disorder (σ_2).

Size (nm)	N_2 (TRANS)	$2\sigma_2^2$ (TRANS)	N_2 (CEY)	$2\sigma_2^2$ (CEY)
Standard	12.00	0.01221	11.82	0.01281
17.3	11.70	0.01298	11.65	0.01291
12.5	11.67	0.01298	11.27	0.01294
9.8	11.38	0.01348	10.76	0.01341

of the population and disorder parameter (σ) of the corresponding cell, we can have an indication of enhancement of Ni deficiency as well as static disorder, as we make particle size smaller. The data acquired with TRANS mode, give very small variations as shown in the inset of Fig. 2 in comparison to CEY mode. One has to remember that, TRANS mode gives the variation in overall (surface+bulk) parameters while CEY mode gives mostly (not "only" because our particle sizes are less than typical information depth of CEY mode but we get most of the surface information because of exponential decaying nature of signal as mentioned above) near-surface region[55] information. So the small variations observed *in TRANS* mode (even if it is not surface sensitive) can actually be attributed to near-surface region. These observations strongly suggest that a different behavior of Ni vacancies and static disorder parameters near the surface and inside the bulk of the particles.

To be quantitative, we have performed the structural refinement to obtain the coordination numbers in second (Ni-Ni) coordination cell. The value of first cell (Ni-O) population has been fixed to stoichiometric value 6 as per previous understandings, mentioned in the introduction. The results are tabulated in Table I and two-cell fitting is presented in Fig. 3. Here we see consistent changes in the second cell coordination numbers in data taken with CEY mode as well as TRANS mode. As expected, the variations in TRANS mode are found to be smaller than corresponding CEY mode. Also note that, as the particle size decreases, TRANS mode starts to give smaller coordination numbers due to larger surface contribution, as TRANS mode gives the overall information as mentioned above. However in all cases, the numbers obtained with CEY mode considerably smaller than corresponding TRANS mode due to near-surface sensitivity and enhancement of effective surface contribution with reduction in particle size. For example, we get 1.5% Ni vacancy for even standard (large grain-size) sample measured with CEY mode as compared to 0.0% in TRANS mode, showing that the combination of TRANS and CEY modes can really be used to separate out surface and bulk contributions. The maximum vacancy concentration has been found to be 10.3% (CEY) for the smallest (9.8 nm) particle. The corresponding value with TRANS mode reads 5.2% (the overall vacancy concentration). From these observations, we can conclude that there exists a definite vacancy-distribution pattern over whole particle volume. The near-surface region of particles contains a larger amount of vacancies, compared to the bulk or core of particles. Our observations on these particular sample set show that the changes in overall vacancy concentrations come through high surface contribution for the nanoparticles. For larger particle size, the vacancy concentration starts to merge within different mode due to very small surface contribution not from the bulk. From these considerations, we can develop a core-shell model for the vacancy distribution, where shell contains a larger number of vacancies compared to core with very little changes in core vacancies for different particles. This is possibly because during the preparation, a vacancy migration occurs from the core to the near-surface region for all particles. Apart from the coordination number changes, we also observe a change in static disorder. As we reduce particle size it increases considerably, as can be seen from Table I.

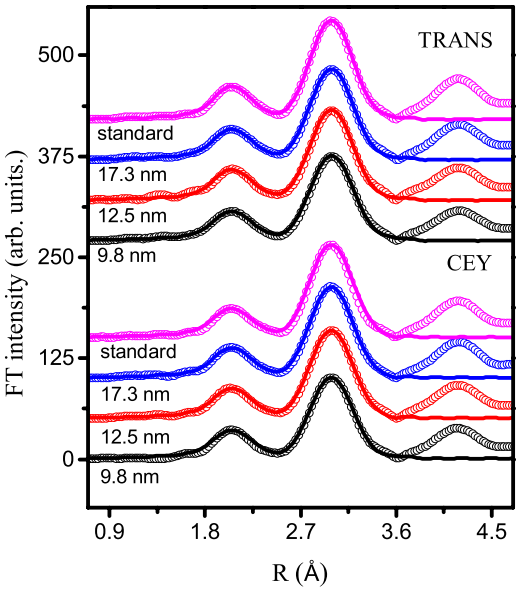

FIG. 3. (Color online) Two cell fits in *R* space for the data taken with TRANS and CEY modes.

B. Development of core-shell magnetic model

Now coming back to magnetic behavior of the nanoparticles, in Fig. 4, we show the hysteresis loops measured at 5 K for three different particle sizes, the smallest (9.8 nm), largest (200 nm), and one in between them (12.5 nm). Both zero-field-cooled (ZFC) and field-cooled (FC) data are presented for the nanoparticles. The nature of these loops is very similar to the observation in Fig. 1 of Ref. 29. In accordance with our structural core-shell model, let us assume (at least for the time being) two magnetic phases are associated, one with core and another with shell. The nonsaturating nature of the loops suggests the presence of antiferromagnetic phase. Now, from the nature of *M-H* plot of the standard sample [see inset of Fig. 4(b)] and the vacancy distribution (very small vacancy concentration 1.5%, which reside on near-surface region), we can be sure that core regions of all particles (containing no or very less concentration of vacancies), behave like antiferromagnet. So, if we subtract this contribution from the overall behavior, we will have an idea about the other phase. This is done in the same way, as done previously[39] to get saturation magnetic moment M_S. One such plot is shown in the inset of Fig. 4(a) for the smallest

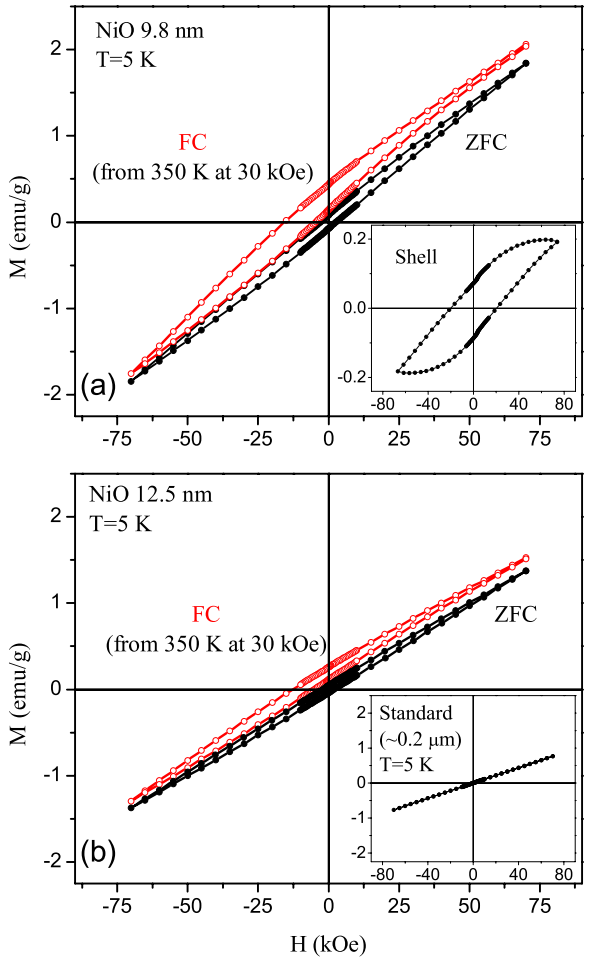

FIG. 4. (Color online) Hysteresis loops at 5 K for (a) 9.8 nm and (b) 12.5 nm with ZFC (solid symbol) and FC (open symbol) from 350 K at 30 kOe. Inset (a) shows shell contribution after subtracting antiferromagnetic core contribution for ZFC loop of 9.8 nm particle. Inset (b) shows *M-H* curve for standard (antiferromagnetic) sample.

particle. The obtained values are M_S(9.8 nm)=0.19 emu/g and M_S(12.5 nm)=0.09 emu/g. Thus, value of M_S increases with reduction in particle size [or with increasing vacancy concentration (see Table I)] as demonstrated in very details in previous studies. Now, let us look at the loop shift upon field cooling. It is evident from Fig. 4 that ZFC loops are symmetric around the origin whereas 30 kOe FC loops are strongly displaced from the origin and also broadened. Apart from the exchange shift H_E, there also exist vertical shift which indicates that some part of the contributing moments are frozen to field direction (while field cooling at 30 kOe). The estimated values of H_E are, H_E(9.8 nm) =5.1 kOe and H_E(12.5 nm)=3.5 kOe, so in our case, H_E increases with increasing vacancy concentration. However it is not always true, in the limit of very small particle size (with associated very high vacancy concentration due to large surface contribution), virtually the shell magnetism dominates with vanishing core contribution. In that regime, H_E no longer increases with decreasing particle size, as we will discuss in subsequent paragraphs.

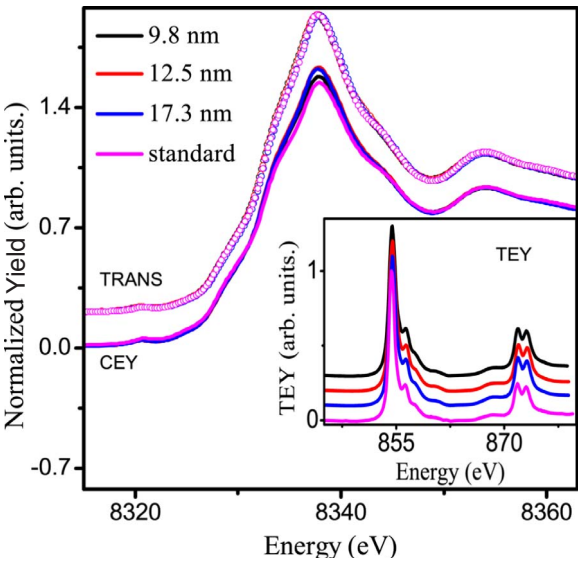

FIG. 5. (Color online) Ni *K*-edge XANES spectra for different nanoparticles (main panel) along with Ni L_{23} (inset) showing the absence of any Ni^{3+} trace.

Along with our magnetic observations and the observations that already exist in literature, we address the following unresolved issues which need some attention to explain within a suitable model. (a) The NiO nanoparticles show a large magnetic moment[29] as sizes become smaller than hundred of nanometer. (b) Observation of spin-glass behavior[33,39] with a broader peak T_p (freezing temperature) in the ZFC curve. (c) Observation of a exchange bias phenomenon, which is responsible for the shifted hysteresis loop after field cooling, with a large loop shift (H_E, the exchange bias field) have been reported for the intermediate sized particle.[29,39] As mentioned earlier the Ni^{3+} ions can play a vital role in determining particle magnetic moment. To check the vacancy induced oxidation state of the Ni ions, most probably NiO nanoparticle is the best system in the sense that it contains a larger amount of Ni vacancies. We can check, the trace of Ni^{3+} ion (if it is present) by observing the absorption (XANES) spectra in Ni *K* edge as well as Ni L_{23} edge. We show the Ni *K*-edge spectra in both CEY and TRANS mode as well as Ni L_{23} in Fig. 5. We do not see any shift in energy between different spectra in Ni *K* edge XANES. Also the spectral shape[44] of the Ni L_{23} edge suggest that Ni ions in NiO nanoparticles remain in a 2+ state and high spin electronic configuration. Thus we exclude the possibility of the effect Ni^{3+} ion on observed large magnetic moment.

Before we proceed further, it is important to discuss the commonly accepted mechanism which is responsible for the observed ferromagnetic behavior of nonmagnetic oxides, in brief. The local magnetic moment in these systems arises as an effect of cation vacancy. The cation vacancy polarizes the surrounding ligand atoms which act as a localized magnetic moment around the vacancy. The ferromagnetic interaction between two such localized moment give rise to a collective ferromagnetic behavior. To establish the collective ferromagnetic behavior, it has been shown[16] that there need a minimum vacancy concentration depending on the crystal struc-

ture of the material involved. The other important parameter to determine the magnitude of local magnetic moment is the charge state of vacancy. For example, in case of HfO_2,[16] if the Hf vacancy occurs in (4−) charge state then the induced local magnetic moment will be zero and one would not expect any collective ferromagnetic properties. For neutral vacancy, the induced local magnetic moment will be maximum. Thus the charge state of the vacancy is also responsible for the strength or observed total magnetic moment of the system.

This model of nonmagnetic system can be extended suitably for the case of antiferromagnetic nanoparticles to explain the observed magnetic behavior accounting the host (antiferromagnetic) induced effect, in addition. The effect of cation vacancy on electronic structure and magnetic properties of transition-metal mono-oxide has been studied by many groups.[9,19,56] The relevant outcomes of these studies are as follows. The introduction of a neutral Ni vacancy in either sublattice results in hole doping on the surrounding ligand oxygen atom $2p$ states. The overall magnetic nature of the system is still antiferromagnetic but the system behaves like a half metal. We point out that by removing one Ni atom from one of the sublattices (up and down) causes an uncompensated moment (which is equal to one Ni moment) that must be compensated by a suitable equivalent moment originated around the vacancy site (over the surrounding ligand atoms) since the net magnetic moment of the system is zero. It is known that if one removes the Ni atom from up sublattice, the resulting hole will arise in the oxygen $2p$ spin-down channel. From these considerations one can think, as if there is a local moment at the vacancy site with the same moment and direction as removed Ni atom. Also while modeling, we have to keep in mind that unlike nonmagnetic system, the antiferromagnetic system posses a variety of exchange interactions and whose strength depend on the lattice parameter[57] while it is on surface or bulk.[58] The important effects of charge state also one has to take into account. From literatures we see that for the case of NiO, the Ni vacancy could be in singly, doubly, or mixed charge states.[12] Also, surface could have effect in determining the charge state, so one should consider the more general case, assuming all charge states are possible.

To see, how our structural core-shell model reflects in its magnetic properties, we point out the following correspondences. (a) The large magnetic moment can be associated with the large Ni vacancy concentration with the reduction in particle size. This experimental vacancy concentration saturates to some value (like 1.5%) as we keep on increasing the particle size. This agrees very well with the experimental observation of total magnetic moment for the particles with sizes only in the nanoscale range (less than 100 nm) where the vacancy concentration varies with size and also the total magnetic moment. (b) As it is evident from our EXAFS studies, even in the nanoscale region we see hardly any changes in the vacancy concentration inside the core of the particle, all changes happening on the near-surface region. So, it agrees very well with the assumption that the core of the particle behave like its original magnetic phase[39] (antiferromagnetism) and we attribute the experimental observation of spin-glass behavior to the near-surface region, the effect is merely due to vacancy induced, enhanced surface disorder, and different surface anisotropy as compared to core. The broader distribution of T_p may come from the particle size distribution but there exist another mechanism which might be more important. This possibly comes because of the distribution of vacancies over the whole particle region. It is most likely that the surface high vacancy concentration falls to its core value continuously (very rapidly as expected from our EXAFS analysis) without any sharp transition. The quasimagnetic phases associated with this kind of vacancy distribution can give rise to a broader T_p. The possible origin of spin-glass phase associated with shell will be discussed at the end. (c) The observed field-cooled loop shift and related phenomenon can come from the exchange coupling between these two, core (antiferromagnetic) and shell (spin-glass) magnetic phases. In the limit of very small (say 3 or 5 nm) particle size, the surface contribution is so much that core contribution becomes negligible and for a larger particle (say 80 or 90 nm) core contribution become significant enough and surface has relatively lesser contribution as compared to very small particle. These competitions between core and shell contributions determine the strength of the exchange phenomenon which will be maximized for an optimal value. That is why, one observes large loop shift for intermediate particle size rather than very small or large particle size within the nanoscale. So the total observed magnetic moment is monotonic function of particle size (as total vacancy concentration) but the loop shift or exchange bias phenomenon is not monotonic with particle size because it strongly depends on the vacancy distribution within the core and shell region.

Before we discuss about the origin of shell magnetism, we would like to comment about the importance of material synthesis condition in determining over all magnetic behavior. Based on our literature survey, we have an impression that the exact association of magnetic properties (for an example, magnetic moment) with sizes sometimes can be misleading and it may not be reproducible. All that matters, are not only preparation temperature but also many other parameters such as capping agent, cooling rate, sample morphology, and surrounding atmospheric conditions even if the particle sizes are kept fixed for each case. These parameters actually control the vacancy distribution over the particle volume in different way, giving different sorts of results.

C. Origin of the shell magnetism

Now we would like to discuss about the possible origin of the shell magnetism. In Fig. 6, we show the situation, schematically in two dimensions. The nickel and oxygen lattice sites are presented by red (dark gray) and light gray small circles, respectively. The spin state of central Ni atoms (of squares) is given at the bottom. The vacancies in up/down sublattices are presented by void (white) regions at Ni sites. The induced moments at surrounding oxygen atoms are presented by small arrows. The overall moments at vacancy sites are presented by big arrows whose magnitude depends on the charge state (q) of vacancies.

(a) $q=0$ case: as discussed earlier, a neutral Ni vacancy introduces two holes in the surrounding ligand $2p$ state in

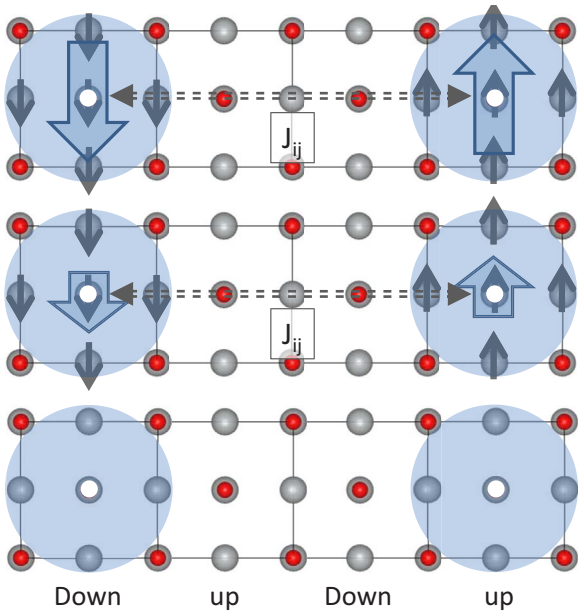

FIG. 6. (Color online) The schematic presentation of proposed model for vacancy induced shell magnetism (see text for details).

such a way that it is introduced in spin-down channel if the Ni atom is removed from the up sublattice. That means induced moment will have a definite direction depending on the vacancy site (see Fig. 6, top). Now see the figure, where we show two such kind of vacancies, one in down sublattice (left) and other is in up sublattice (right). It is clear that due to host induced effect the moments are antiparallel. But, there may exist another interaction J_{ij} (in a similar way of nonmagnetic system) which will try to make them parallel. J_{ij} must be dependent on the distance between two such moments (in turns, on vacancy concentration). Along with these competing interactions and randomness of vacancy sites, enhanced surface disorder, make the overall system to behave as a spin glass.

(b) $q=-2$ case: for this case, there will not be any induced magnetic moment around the vacancy site (see Fig. 6, bottom) but system posses a net magnetic moment due to two-sublattice unconsenting moment (coming from vacancies and intrinsic surface effect). Along with surface roughness, disorder, and vacancy-site randomness, the system behaves as a spin glass.

(c) $q=-1$ or mixed case: this is the most reliable mechanism which combines both of above two and consistent with experimental findings. In this case, the induced magnetic moment is reduced to its half value as compared with (a) (see Fig. 6, middle).

IV. SUMMARY

In summary, NiO nanoparticles of different particle sizes have been prepared in a similar way, as done in most of the relevant works. A detailed surface and bulk vacancy characterization have been performed using EXAFS technique. Our observation and analysis show that there exist a definite pattern of vacancy distribution over the particle volume which can be described within a core-shell model. The importance of this vacancy distribution for different particle sizes on their magnetic properties has been discussed excluding the contribution coming from Ni^{3+} ions. Here, we extend the idea about the vacancy induced magnetism of nonmagnetic system to antiferromagnetic system. We argue that by accounting the host induced effect along with vacancy-vacancy interaction can give a suitable explanation for the observed spin-glass behavior. We demonstrate that the structural core-shell model identically reflects in its magnetic behavior resembling the system as a core-shell exchange bias system. The core retains its original magnetic phase and shell behaves as spin glass. The distribution of vacancies determines the nature of size-dependent exchange bias strength, which is not monotonic with particle size as total magnetic moment in nanometer scale. Though the experiments were performed on NiO but our understanding should be valid for all other antiferromagnetic oxide nanoparticles.

ACKNOWLEDGMENTS

The work was partly supported by the International Center for Theoretical Physics (ICTP), Trieste and the Department of Science and Technology (DST), India along with the Italian Ministry of Foreign Affairs for Synchrotron Radiation Studies. Authors acknowledge the friendly help and discussion of Luca Olivi, Stefano Nannarone, and other scientific fellows of XAFS and BEAR beamlines of the Elettra Synchrotron Center during measurements. Authors thankfully acknowledge K. S. Priolkar and P. S. Devi for various fruitful discussions and S. Hazra for XRD measurements.

*krishna.menon@saha.ac.in

[1] B. Zhao, X.-K. Ke, J.-H. Bao, C.-L. Wang, L. Dong, Y.-W. Chen, and H.-L. Chen, J. Phys. Chem. C **113**, 14440 (2009).
[2] J. Park, E. Kang, S. U. Son, H. M. Park, M. K. Lee, J. Kim, K. W. Kim, H.-J. Noh, J.-H. Park, C. J. Bae, J.-G. Park, and T. Hyeon, Adv. Mater. (Weinheim, Ger.) **17**, 429 (2005).
[3] M. C. A. Fantini, F. F. Ferreira, and A. Gorenstein, Solid State Ionics **152-153**, 867 (2002).
[4] G. Mattei, P. Mazzoldi, M. L. Post, D. Buso, M. Guglielmi, and A. Martucci, Adv. Mater. (Weinheim, Ger.) **19**, 561 (2007).
[5] J. A. Dirksen, K. Duval, and T. A. Ring, Sens. Actuators B **80**, 106 (2001).
[6] S. I. Kim, J. H. Lee, Y. W. Chang, S. S. Hwang, and K.-H. Yoo, Appl. Phys. Lett. **93**, 033503 (2008).
[7] J. Caruge, J. E. Halpert, V. Bulovic, and M. G. Bawendi, Nano Lett. **6**, 2991 (2006).
[8] A. M. Ferrari C. Pisani, F. Cinquini, L. Giordano, and G. Pacchioni, J. Chem. Phys. **127**, 174711 (2007).
[9] S. Park, H. S. Ahn, C. K. Lee, H. Kim, H. Jin, H. S. Lee, S. Seo, J. Yu, and S. Han, Phys. Rev. B **77**, 134103 (2008).

[10] S. Lany, J. Osorio-Guillén and A. Zunger, Phys. Rev. B **75**, 241203(R) (2007).
[11] W. Jang, Y.-M. Lu, W.-S. Hwang, T.-L. Hsiung, and H. P. Wang, Appl. Phys. Lett. **94**, 062103 (2009).
[12] J. Nowotny and A. Sadowski, J. Am. Ceram. Soc. **62**, 24 (1979).
[13] Z. Grezesik and S. Mrowec, Pol. J. Chem. **79**, 907 (2005).
[14] M. Venkatesan, C. B. Fitzgerald, and J. M. D. Coey, Nature (London) **430**, 630 (2004).
[15] Y. Wang, Y. Huang, Y. Song, X. Zhang, Y. Ma, J. Liang, and Y. Chen, Nano Lett. **9**, 220 (2009).
[16] J. Osorio-Guillén, S. Lany, S. V. Barabash, and A. Zunger, Phys. Rev. B **75**, 184421 (2007).
[17] G. Bouzerar and T. Ziman, Phys. Rev. Lett. **96**, 207602 (2006).
[18] V. Fernandes, R. J. O. Mossanek, P. Schio, J. J. Klein, A. J. A. de Oliveira, W. A. Ortiz, N. Mattoso, J. Varalda, W. H. Schreiner, M. Abbate, and D. H. Mosca, Phys. Rev. B **80**, 035202 (2009).
[19] A. Soon, X. Y. Cui, B. Delley, S. H. Wei, and C. Stampfl, Phys. Rev. B **79**, 035205 (2009).
[20] G. Rahman, V. M. García-Suárez, and S. C. Hong, Phys. Rev. B **78**, 184404 (2008).
[21] O. V. Yazyev, Phys. Rev. Lett. **101**, 037203 (2008).
[22] C. Madhu, A. Sundaresan and C. N. R. Rao, Phys. Rev. B **77**, 201306(R) (2008).
[23] P. Dev, Y. Xue, and P. Zhang, Phys. Rev. Lett. **100**, 117204 (2008).
[24] A. Sundaresan, R. Bhargavi, N. Rangarajan, U. Siddesh and C. N. R. Rao, Phys. Rev. B **74**, 161306(R) (2006).
[25] N. H. Hong, J. Sakai, N. Poirot, and V. Brizé, Phys. Rev. B **73**, 132404 (2006).
[26] J. Osorio-Guillén, S. Lany, S. V. Barabash, and A. Zunger, Phys. Rev. Lett. **96**, 107203 (2006).
[27] I. S. Elfimov, S. Yunoki, and G. A. Sawatzky, Phys. Rev. Lett. **89**, 216403 (2002).
[28] C. Das Pemmaraju and S. Sanvito, Phys. Rev. Lett. **94**, 217205 (2005).
[29] R. H. Kodama, S. A. Makhlouf, and A. E. Berkowitz, Phys. Rev. Lett. **79**, 1393 (1997).
[30] S. A. Makhlouf, F. T. Parker, F. E. Spada, and A. E. Berkowitz, J. Appl. Phys. **81**, 5561 (1997).
[31] D. Tobia, E. Winkler, R. D. Zysler, M. Granada, and H. E. Troiani, Phys. Rev. B **78**, 104412 (2008).
[32] L. Li, L. Chen, R. Qihe, and G. Li, Appl. Phys. Lett. **89**, 134102 (2006).
[33] S. D. Tiwari and K. P. Rajeev, Phys. Rev. B **72**, 104433 (2005).
[34] M. A. Morales, R. Skomski, S. Fritz, G. Shelburne, J. E. Shield, M. Yin, S. OBrien, and D. L. Leslie-Pelecky, Phys. Rev. B **75**, 134423 (2007).
[35] E. Winkler, R. D. Zysler, M. Vasquez Mansilla, D. Fiorani, D. Rinaldi, M. Vasilakaki, and K. N. Trohidou, Nanotechnology **19**, 185702 (2008).
[36] E. L. Salabaş, A. Rumplecker, F. Kleitz, F. Radu, and F. Schüth, Nano Lett. **6**, 2977 (2006).
[37] T. Park, G. C. Papaefthymiou, A. J. Viescas, A. R. Moodenbaugh, and S. S. Wong, Nano Lett. **7**, 766 (2007).
[38] W.-B. Zhang, N. Yu, W.-Y. Yu, and B.-Y. Tang, Eur. Phys. J. B **64**, 153 (2008).
[39] S. A. Makhlouf, H. Al-Attar, and R. H. Kodama, Solid State Commun. **145**, 1 (2008).
[40] A. Sundaresan and C. N. R. Rao, Nanotoday **4**, 96 (2009).
[41] M. J. Benitez, O. Petracic, E. L. Salabas, F. Radu, H. Tuysuz, F. Schuth, and H. Zabel, Phys. Rev. Lett. **101**, 097206 (2008).
[42] S. Jacobs and C. P. Bean, in *Magnetism*, edited by G. T. Rado and H. Suhl (Academic, New York, 1963), Vol. III, p. 294.
[43] M. J. Tomellini, J. Electron Spectrosc. Relat. Phenom. **58**, 75 (1992).
[44] L. Soriano, M. Abbate, J. Vogel, J. C. Fuggle, A. Fernández, A. R. González-Elipe, M. Sacchi, and J. M. Sanz, Chem. Phys. Lett. **208**, 460 (1993).
[45] L. Soriano, A. Gutierrez, I. Preda, S. Palacin, J. M. Sanz, M. Abbate, J. F. Trigo, A. Vollmer, and P. R. Bressler, Phys. Rev. B **74**, 193402 (2006).
[46] M. Gruyters, Phys. Rev. B **79**, 134415 (2009).
[47] T. Girardeau, J. Mimault, M. Jaouen, P. Chartier, and G. Tourillon, Phys. Rev. B **46**, 7144 (1992).
[48] M. E. Kordesch and R. W. Hoffman, Phys. Rev. B **29**, 491 (1984).
[49] S. Zheng, S. Hayakawa, and Y. Gohshi, J. Electron Spectrosc. Relat. Phenom. **87**, 81 (1997).
[50] B. Ravel and M. J. Newville, Synchrotron Radiat. **12**, 537 (2005).
[51] J. J. Rehr and R. C. Albers, Rev. Mod. Phys. **72**, 621 (2000).
[52] P. A. Lee, P. H. Citrin, P. Eisenberger, and B. M. Kincaid, Rev. Mod. Phys. **53**, 769 (1981).
[53] S. Tomic, B. G. Searle, A. Wander, N. M. Harrison, A. J. Dent, J. F. W. Mosselmans, and J. E. Inglesfield, New Tools for the Analysis of EXAFS: The DL_EXCURV Package, CCLRC Technical Report DL-TR-2005–001, 2005.
[54] E. A. Stern, D. E. Sayers, and F. W. Lytle, Phys. Rev. B **11**, 4836 (1975).
[55] T. Nonaka, C. Okuda, Y. Seno, K. Koumoto, and Y. Ukyo, Ceram. Int. **34**, 859 (2008).
[56] D. Ködderitzsch, W. Hergert, Z. Szotek, and W. M. Temmerman, Phys. Rev. B **68**, 125114 (2003).
[57] W. B. Zhang, Y. L. Hu, K. L. Han, and B. Y. Tang, Phys. Rev. B **74**, 054421 (2006).
[58] D. Ködderitzsch, W. Hergert, W. M. Temmerman, Z. Szotek, A. Ernst, and H. Winter, Phys. Rev. B **66**, 064434 (2002).